AGU PUBLICATIONS

JGR

Journal of Geophysical Research: Atmospheres

RESEARCH ARTICLE
10.1002/2016JD025482

Key Points:
- High-latitude dust sources in the Northern Hemisphere contribute substantially to mineral dust in the Arctic and global dust load
- Results show a difference between seasonal cycle of dust load and dust deposition in the Arctic
- The source region of dust deposited on the Greenland ice sheet changes with altitude

Correspondence to:
C. D. Groot Zwaaftink,
cgz@nilu.no

Citation:
Groot Zwaaftink, C. D., H. Grythe, H. Skov, and A. Stohl (2016), Substantial contribution of northern high-latitude sources to mineral dust in the Arctic, *J. Geophys. Res. Atmos.*, *121*, 13,678–13,697, doi:10.1002/2016JD025482.

Received 8 JUN 2016
Accepted 27 OCT 2016
Accepted article online 2 NOV 2016
Published online 25 NOV 2016

Substantial contribution of northern high-latitude sources to mineral dust in the Arctic

C. D. Groot Zwaaftink[1], H. Grythe[1,2,3], H. Skov[4], and A. Stohl[1]

[1]NILU - Norwegian Institute for Air Research, Kjeller, Norway, [2]Department of Environmental Science and Analytical Chemistry, Atmospheric Science Unit, Stockholm University, Stockholm, Sweden, [3]Air Quality Research, Finnish Meteorological Institute, Helsinki, Finland, [4]Arctic Research Center, Department of Environmental Science, Aarhus University, Roskilde, Denmark

Abstract In the Arctic, impurities in the atmosphere and cryosphere can strongly affect the atmospheric radiation and surface energy balance. While black carbon has hence received much attention, mineral dust has been in the background. Mineral dust is not only transported into the Arctic from remote regions but also, possibly increasingly, generated in the region itself. Here we study mineral dust in the Arctic based on global transport model simulations. For this, we have developed a dust mobilization scheme in combination with the Lagrangian particle dispersion model FLEXPART. A model evaluation, based on measurements of surface concentrations and annual deposition at a number of stations and aircraft vertical profiles, shows the suitability of this model to study global dust transport. Simulations indicate that about 3% of global dust emission originates from high-latitude dust sources in the Arctic. Due to limited convection and enhanced efficiency of removal, dust emitted in these source regions is mostly deposited closer to the source than dust from for instance Asia or Africa. This leads to dominant contributions of local dust sources to total surface dust concentrations (~85%) and dust deposition (~90%) in the Arctic region. Dust deposition from local sources peaks in autumn, while dust deposition from remote sources occurs mainly in spring in the Arctic. With increasing altitude, remote sources become more important for dust concentrations as well as deposition. Therefore, total atmospheric dust loads in the Arctic are strongly influenced by Asian (~38%) and African (~32%) dust, whereas local dust contributes only 27%. Dust loads are thus largest in spring when remote dust is efficiently transported into the Arctic. Overall, our study shows that contributions of local dust sources are more important in the Arctic than previously thought, particularly with respect to surface concentrations and dust deposition.

1. Introduction

Aeolian transport of mineral dust ($<20\,\mu m$; see later) has been a topic of research for decades. A large part of the interest in aeolian dust is driven by the large consequences it may have. Mineral aerosols bring nutrients to oceanic and terrestrial ecosystems, often at large distances from the dust source regions [e.g., *Okin et al.,* 2004; *Moore et al.,* 2004]. Air quality can be heavily decreased causing issues for human health [e.g., *Griffin and Kellogg*, 2004]. Clouds can be affected by dust particles as they serve as ice and cloud condensation nuclei (CCN) allowing ice and liquid droplet formation [e.g., *Yin et al.,* 2002; *Koehler et al.,* 2010]. And, not in the least, the particles absorb and reflect solar radiation. This can affect the radiation balance of the atmosphere, as well as the surface energy balance. The presence of mineral dust may be particularly relevant for snow- or ice-covered regions, where dust may decrease the surface albedo [e.g., *Warren and Wiscombe*, 1980; *Stone et al.,* 2007]. Increasing amounts of impurities in Arctic snow have been suggested to originate from local sources that experience a seasonal snow cover [*Dumont et al.,* 2014]. Earlier melt of the seasonal snow cover may thus affect dust mobilization and subsequently snow and ice albedo, which is important since for instance already small decreases in fresh snow albedo of 1% may lead to surface mass losses of $27\,Gt\,yr^{-1}$ from the Greenland ice sheet [*Dumont et al.,* 2014].

Dust transport models have been developed and used for local and global dust transport simulations [e.g., *Tegen and Fung*, 1994; *Liu et al.,* 2003; *Uno et al.,* 2003; *Zender et al.,* 2003a; *Huneeus et al.,* 2011]. Naturally, aeolian dust research has focused on areas where dust is present in abundance, such as the Sahara or Gobi desert. However, large availability of dust is evident in the Arctic as well [e.g., *Fristrup,* 1953; *Arnalds*, 2010; *Dagsson-Waldhauserova et al.,* 2014a; *Bullard et al.,* 2016]. These high-latitude dust sources have also been

identified in model studies [e.g., *Mahowald et al.,* 1999; *Andersen et al.,* 1998]. Nonetheless, they have been given relatively little attention in or have even been removed from global simulations [e.g., *Zender et al.,* 2003a]. The information on transport of dust to and in the Arctic is therefore limited. *Rahn et al.* [1977] attributed elevated Arctic haze layers to transport of dust from Asia. *Andersen et al.* [1998] estimated contributions of dust from different source regions, defined by their latitude, to deposition on the polar ice caps under glacial and interglacial conditions. Results, however, overestimate contributions from lower latitudes on the Northern Hemisphere [*Andersen et al.,* 1998]. *Fan* [2013] modeled mineral dust concentrations in the Arctic and investigated the impact of dust on cloud formation. It was pointed at possible origins of dust in the Sahara and Asia. An underestimation of modeled dust concentrations in autumn was suggested to be due to a lack of local dust sources in the model. Model simulations by *Lambert et al.* [2015] suggested that besides Asian dust, also Siberian and Alaskan sources may have been potential contributors to dust in Greenland ice cores in the Last Glacial Maximum. Generally, it appears that past model studies have emphasized the episodic long-range transport of dust from major desert areas to the Arctic but have paid little attention to Arctic or high-latitude sources of dust.

Much information on dust sources and deposition amounts can also be retrieved from snow samples and ice cores. Especially in combination with transport modeling, these help to recognize important dust source regions. In ice core studies, a seasonal variation of dust deposition has been detected early [e.g., *Hamilton and Langway*, 1967], and this characteristic has been used to date ice core layers [e.g., *Ram and Koenig*, 1997]. Snow samples from the Canadian Ice Cape were used by *Zdanowicz et al.* [1998] to analyze variations of dust deposition and allocate possible source regions. Some evidence of peaks of deposition in late winter-spring and late summer-fall was found. Relatively small particles sizes in late winter-spring and larger particle sizes in late summer-fall lead to the conclusion that the two peaks are related to distal and proximal source regions, respectively [*Zdanowicz et al.,* 1998]. A comparison of the composition of dust in ice cores at Summit, Greenland, to dust from possible sources indicated that probable sources are found in eastern Asia. Furthermore, the dust deposited during the last full glacial could not be linked to sources in the Sahara or midcontinental United States [*Biscaye et al.,* 1997]. Additionally, chemical analysis of snow samples taken in Greenland also indicated that dust deposition varies seasonally [*Bory et al.,* 2002, 2003a]. In these studies it was concluded that the main source region of dust deposited here is eastern Asia. A comparison with potential source areas in Asia indicated that two different source regions are dominant depending on the season. Conclusions of such studies depend on the completeness of potential source areas taken into account. *Biscaye et al.* [1997] did not include dust from high latitudes, except Alaska, among their potential source areas. From chemical analysis of a set of ice cores on the Greenland ice sheet it was concluded that elevated sites are influenced by Asian dust and sites located closer to the edge and at lower altitude are influenced by proximal sources [*Bory et al.,* 2003b].

Combinations of aerosols sample studies and trajectory analysis can provide additional confidence in determining source areas. Such a study revealed that also Saharan dust can reach Summit, Greenland [*VanCuren et al.,* 2012]. Transport of Asian dust to the Arctic has been confirmed in case studies [*Rahn et al.,* 1977; *Huang et al.,* 2015; *Kang et al.,* 2015]. While case studies give valuable information on possible transport routes, they cannot quantify the relative contributions of all potential dust sources.

We aim to investigate seasonal variation of Arctic dust deposition and concentration and distinguish contributions of local versus remote sources. The Lagrangian model FLEXPART [*Stohl et al.,* 1998, 2005] has proven to be a valuable model in estimating air pollution transport in the Arctic and defining source regions [*Stohl et al.,* 2002; *Eckhardt et al.,* 2003; *Stohl*, 2006; *Hirdman et al.,* 2010; *Stohl et al.,* 2013]. Especially for the Arctic region, *Stohl* [2006] could reveal important transport mechanisms based on FLEXPART simulations. The model has also been used for dust transport calculations [*Sodemann et al.,* 2015], but an enhanced dust mobilization scheme that can be used in combination with FLEXPART will be introduced in this manuscript. We will evaluate the performance of FLEXPART in modeling dust transport based on observations of surface concentration and deposition at sites remote from dust sources. We will then focus on dust deposition and dust loading in the Arctic in section 3, showing that high-latitude dust sources in the Northern Hemisphere contribute substantially to dust loads and especially dust deposition in the Arctic. We will refer to the region north of 60°N as "near Arctic" and north of 80°N as "high Arctic".

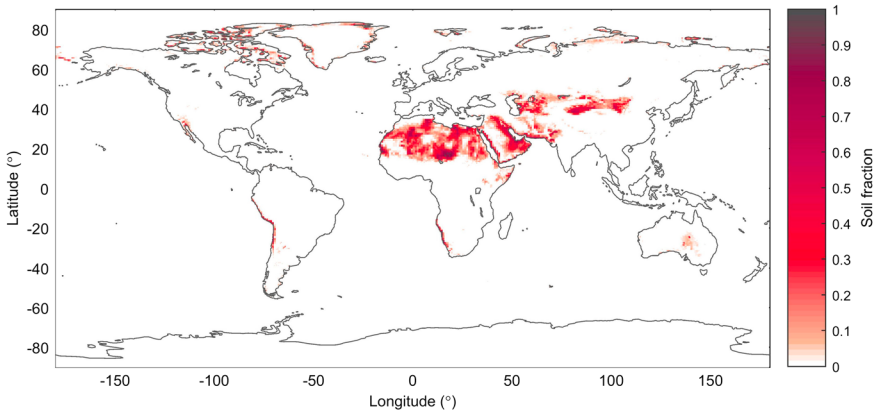

Figure 1. Erodible soil fraction after scaling according to equation (1).

2. Model and Data

2.1. FLEXDUST

The Lagrangian particle dispersion model FLEXPART [*Stohl et al.,* 1998] has been used earlier to describe dust transport events in the Sahara region [*Sodemann et al.,* 2015]. However, for the current purpose, the previous emission module that relied on fixed descriptions of threshold friction velocity appeared inadequate since we now apply the model on a global scale. Nonetheless, we also have to consider that information on soil properties is limited and advanced physical models of dust mobilization are not globally applicable. The current dust emission module, called FLEXDUST, relies on simple formulations common in global dust transport models. To improve mineral dust, quantifications in the Arctic special attention was given to soil fraction estimates at high latitudes.

A first step is to know where mineral dust is available; we thus need to know the bare soil fraction. Land cover data are a crucial part in modeling dust emission. We here used the Global Land Cover by National Mapping Organizations (version 2 [*Tateishi et al*., 2014]) at a 15 arcsec pixel^{-1} resolution. As a source for dust emission, we included both land cover classes bare soil (sand) and partly vegetated areas. For partly vegetated areas, we determine available soil fraction by subtracting the vegetation cover fraction as used by the European Centre for Medium-Range Weather Forecasts (ECMWF) [*Boussetta et al.,* 2013]. Additionally, as Iceland is an important high-latitude dust source, we used a land cover data set that describes all bare land regions in Iceland and identifies regions with sandy deserts [*Dagsson-Waldhauserova et al.,* 2014b; *Arnalds,* 2015]. Furthermore, we account for topographic effects. As proposed by *Ginoux et al.* [2001] and further discussed by *Zender et al.* [2003b], sediments are likely to gather in depressions, and those areas should therefore be considered as more favorable for dust emission than elevated terrain. We thus also apply the erodibility scaling (S) according to *Ginoux et al.* [2001]:

$$S = \left(\frac{z_{max} - z_i}{z_{max} - z_{min}} \right)^5 \quad (1)$$

Here z_i is the local elevation and z_{max} and z_{min} are the, respectively, maximum and minimum elevation in a surrounding 10° latitude × 10° longitude area following *Ginoux et al.* [2001]. Note that this large scale will be able to detect large basins but may overshadow smaller glacier valleys. This scale thus needs to be adjusted in case of regional simulations or specific interest in glacier valleys. Moreover, for arid regions the method to parameterize erodibility based on satellite data, as described by *Parajuli et al.* [2014], may, for instance, also be applicable.

The soil fraction available from land cover data is scaled by the erodibility. Applying the assumptions and using the land cover data then finally results in a map of erodible soil fraction (Figure 1).

Due to the inclusion of the topographic scaling factor of *Ginoux et al.* [2001] especially topographic depressions such as the Bodele depression in Africa and coastal areas (e.g., Arabian Peninsula and Greenland) show up as strong source regions for mineral dust (Figure 1).

The initiation of dust emission from these regions may be defined through a threshold friction velocity. In case of aerodynamic entrainment, one important factor influencing the threshold friction velocity for particle mobilization is the particle size [e.g., *Shao and Lu*, 2000]. In aeolian transport, however, particles will not only be aerodynamically entrained but also be ejected by impacting particles, and this form of mobilization is probably more important than aerodynamic entrainment. We may therefore assume that the minimal threshold friction velocity of all particle sizes is determining dust mobilization of the complete size distribution. Empirical expressions of threshold friction velocity described by *Iversen and White* [1982] and *Shao and Lu* [2000] define a minimum threshold for particle sizes of approximately 75 to 100 μm, as also presented by *Kok et al.* [2012]. In our simulations, we assume that in case sand is present in the soil, particles of size 75 μm determine threshold friction velocity u_{*t} using the expression of *Shao and Lu* [2000]:

$$u_{*_t} = \sqrt{A_N\left(\sigma_p g d_p + \frac{\gamma}{\rho d_p}\right)} \tag{2}$$

Here σ_p is the particle to air density ratio, d_p is particle diameter, g is acceleration due to gravity, and ρ is air density. We assume values of $A_N = 0.0123$ and $\gamma = 3 \cdot 10^{-4}\,\mathrm{kg\,s^{-2}}$ according to *Shao and Lu* [2000]. Similar assumptions were made in other global dust transport models, for instance Dust Entrainment and Deposition (DEAD) [*Zender et al.,* 2003a]. For regions where clay or silt is present, but no sand, we assume a particle size of 10 μm to estimate threshold friction velocity. Clay, sand, and silt fractions were obtained from the *Global Soil Data Task* [2014].

Soil moisture can have a limiting effect on dust emission. Building on the parameterization of *McKenna-Neuman and Nickling* [1989] that considered this effect for sand, *Fécan et al.* [1999] derived an expression for all soil types. Recently, *Kim and Choi* [2015] demonstrated the use of satellite observations to parameterize the influence of soil moisture on dust emission on larger scales for bare sand areas. We here use the parametrization derived by *Fécan et al.* [1999]. Using only soil moisture and clay content, influence of capillary forces on threshold for mobilization can be estimated as the ratio of threshold friction velocity for wet (u_{*tw}) and dry (u_{*t}) conditions by

$$\frac{u_{*_{tw}}}{u_{*_t}} = 1 \qquad \left(w < w'\right) \tag{3}$$

$$\frac{u_{*_{tw}}}{u_{*_t}} = \sqrt{1 + 1.21\left(w - w'\right)^{0.68}} \quad \left(w \geq w'\right) \tag{4}$$

Here w is the volumetric water content of the soil (%). Capillary forces start to affect threshold friction velocity once a level w' is reached. This level depends on the clay content

$$w' = 0.17c + 0.0014c^2 \tag{5}$$

where c is the clay content (%). The volumetric water content of the top soil layer is retrieved from the ECMWF operational analysis fields. We are aware of uncertainties in soil moisture modeling that will affect emission estimates. *Grini et al.* [2005] avoided this by using the precipitation data to prohibit dust emission during and after precipitation events instead. That approach, however, did not improve model results. Especially in northern latitudes, soil moisture appeared a better indicator of mobilization threshold as seasonal variations in surface dust concentrations at remote stations were better captured and total emission amounts were closer to other model estimates. This may also be due to recent improvements in the ECMWF soil moisture schemes. Also surface roughness affects dust emission [e.g., *Parajuli et al.,* 2016], yet detailed information on surface roughness and the influence of surface roughness on dust emission on global scales are lacking. Drag partition due to nonerodible obstacles is accounted for as described by *Zender et al.* [2003a] in case of limited soil fraction. We further assume that snow cover (also provided by the ECMWF analysis data) inhibits dust mobilization. In case of thin or patchy snow covers, dust transport, maybe even combined with drifting snow, is possible [e.g., *Bullard et al.,* 2016], but this requires more detailed information of the snow cover than available in global transport models. Frost can both increase threshold friction velocities due to cementing fine particles and ease aeolian transport by breaking aggregates [*Bullard and Austin*, 2011]. This complex process is not accounted for in FLEXDUST.

Once mobilization thresholds are estimated, we need to derive dust emission amounts. These estimates are done based on the following parameterization for the vertical dust flux presented by *Marticorena and Bergametti* [1995]:

$$F = c\alpha\frac{\rho u_*^3}{g}\left(1-\frac{u_{*_t}^2}{u_*^2}\right)\left(1+\frac{u_{*_t}}{u_*}\right) \tag{6}$$

where u_* is friction velocity, c is an added constant scaling factor ($4.8 \cdot 10^{-4}$), and α is the sand blasting efficiency depending on clay fraction. The friction velocity used in FLEXDUST is based on the shear stress data from ECMWF and thus consistent with the FLEXPART simulations. The emitted dust is assumed to have a volume size distribution varying between 0.2 and 18.2 μm based on brittle fragmentation theory according to *Kok* [2011]:

$$\frac{d\ V_d}{d\ ln\ D_d} = \frac{D_d}{c_V}\left[1+\ \mathrm{erf}\left(\frac{\ln\left(D_d/\overline{D_s}\right)}{\sqrt{2}\ln\sigma_s}\right)\right]\exp\left[-\left(\frac{D_d}{\lambda}\right)^3\right] \tag{7}$$

V_d is the normalized volume of dust particles with size D_d. We assume values of 12.62 μm for the normalization constant c_V, 3.0 for the geometric standard deviation σ_s, and propagation distance $\lambda = 12$ μm following *Kok et al.* [2012]. Larger-sized particles are not included in our simulations since the shorter transport distance is not relevant for the scales we consider.

2.2. FLEXPART

Dust transport is calculated with the Lagrangian particle dispersion model FLEXPART [*Stohl et al.*, 1998, 2005] driven with 3-hourly operational meteorological data from ECMWF at 1° × 1° resolution. Dust transport was calculated with this model before, as presented by *Sodemann et al.* [2015]. We use FLEXPART version 10, with a recently developed wet deposition scheme that determines in-cloud and below-cloud scavenging based on cloud information from the ECMWF meteorological data sets [*Grythe et al.*, 2016]. This scheme requires scavenging coefficients for in-cloud and below-cloud scavenging related to particle properties, which represents the efficiency of scavenging processes. Mineral aerosols may initially be insoluble and therefore inefficient CCN. Weathering during transport can, however, change the physical and chemical properties of the particles [*Prospero*, 1999]. A coating, with for instance sulfate, can increase the effectiveness of dust particles as CCN [*Yin et al.*, 2002]. We therefore assume values of 0.45 for CCN and 0.1 for ice nucleation efficiency for small particles (<10 μm) and values of 0.9 and 0.1, respectively, for larger particles. Besides wet deposition, gravitational particle settling [*Näslund and Thaning*, 1991] is also accounted for assuming spherical particle shapes.

For our dust simulations, we use 10 particle size classes of equal size with particle diameters ranging from 0.2 to 18.2 μm, following the size distribution in equation (7). Dust emission rates are calculated on a global grid of 0.5° × 0.5° resolution and with a time resolution of 3 h. Emission releases in FLEXPART were then summed into 6-hourly intervals on 1° resolution. In every grid cell with dust emissions, virtual particles are released in FLEXPART, with the number of particles being proportional to the emitted mass. The simulations cover the years 2010 through 2012 and include over 80 million particles. Particles are carried in the simulation for up to 120 days, after which they are terminated.

2.3. Data

Evaluation of our mineral dust simulations will be based on existing data sets of atmospheric dust concentrations and deposition amounts. *Huneeus et al.* [2011] presented an intercomparison of dust transport models and gathered several measurement data sets on, among others, dust concentration and deposition. Annual dust deposition amounts were retrieved from several sources, such as ice cores, iron deposition, and ocean sediment traps. In our comparison, we include 84 sites presented by *Huneeus et al.* [2011] based on data of *Ginoux et al.* [2001], *Mahowald et al.* [1999], *Mahowald et al.* [2009], *Kohfeld and Harrison* [2001], and *Tegen et al.* [2002]. Surface dust concentrations were retrieved from filter samples and measurements of aluminum concentration (see *Huneeus et al.* [2011] and references therein for more details). Measurements in the Pacific Ocean were done as part of the Sea-Air Exchange program [*Prospero et al.*, 1989] and in the North Atlantic in the Atmosphere/Ocean Chemistry Experiment [*Arimoto et al.*, 1995]. Furthermore, the data set provided by *Huneeus et al.* [2011] included data of 20 sites from the

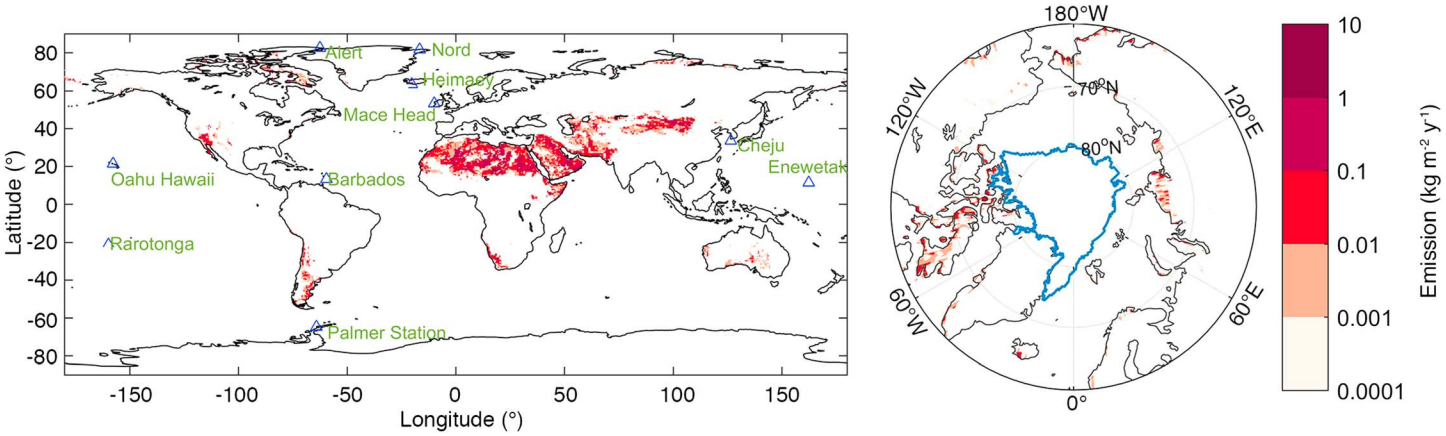

Figure 2. Simulated (left) global and (right) near Arctic annual mean dust emission (kg m^{-2}). The names in the left figure refer to stations with observations of dust concentrations used in section 3.2. The blue line in the right figure represents the sea ice extent in September 2012 [*Fetterer et al.,* 2002].

Rosenstiel School of Marine and Atmospheric Science, University of Miami [*Prospero et al.,* 1989; *Prospero*, 1996; *Arimoto et al.,* 1995]. Our model results will be compared to a part of this surface concentration data set. We chose a set of stations representative for different regions. The following are selected stations and measurement periods: Ragged Point Barbados (May 1984 to July 1998), Cheju (September 1991 to October 1995), Enewetak Atoll (February 1981 to June 1987), Mace Head (August 1988 to August 1994), Oahu Hawaii (January 1981 to July 1995), Palmer Station Antarctica (April 1990 to October 1996), and Rarotonga (March 1983 to June 1994). Station locations are shown in Figure 2.

Furthermore, we include dust surface concentration measurements from Heimaey, Storhofdi (Iceland, years 1997–2002), provided by J. Prospero [*Prospero et al.,* 2012]. We also retrieved dust concentrations from aluminum measurements at Villum Research Station, Station Nord [*Nguyen et al.,* 2013] for the period September 1990 to June 2002 and September 2007 to December 2013 and at Station Alert [*Sirois and Barrie*, 1999] for the years 1980–1994. We assumed a mass ratio of 7.1% to obtain dust concentrations from aluminum concentration measurements. *Nguyen et al.* [2013] estimated that about 50% of aluminum concentrations at Station Nord can be explained by natural sources, while anthropogenic sources account for the other half. We thus have to consider a likely overestimation of observed mineral dust concentrations at Station Nord up to 50%. Especially in summer, we may also expect overestimated dust concentrations due to activities at Station Nord.

Further model evaluation is done based on vertical profiles of dust concentrations in the Arctic. Observations are from the Arctic Research of the Composition of the Troposphere from Aircraft and Satellites (ARCTAS) flight campaigns [*Jacob et al.,* 2010]. We selected all DC8 flights in April and July 2008. From these flights, only data obtained north of 60°N were included in this study. Low-altitude observations near Fairbanks, Barrow, and Prudhoe Bay were removed, in analogy with *Breider et al.* [2014]. We used the same method as *Breider et al.* [2014] to obtain dust concentrations. That is, we assumed a mass ratio of 6.8% to obtain dust concentrations from calcium concentrations. Calcium concentrations were corrected for sea salt based on sodium concentrations using a mass ratio of 4%.

3. Results and Discussion

3.1. Global Dust Emission

Annual dust emission is strongly related to soil fraction available for aeolian transport (see Figure 1). The mere availability of sand, however, is not enough. As described in section 2.1, in FLEXDUST soil moisture and snow cover can decrease dust emission and, above all, dust emission strongly depends on friction velocity. Annual dust fluxes in Figure 2 therefore show a pattern that is somewhat different from the soil fraction map in Figure 1. Largest dust emission fluxes were found in the region of the Bodele depression. Other regions that are clearly large sources of airborne mineral dust are the Gobi desert and the

Table 1. Estimated Relative and Absolute Mean Annual Dust Emission[a]

	Relative Dust Emission (%)	Dust Emission ($Tg\,y^{-1}$)	AEROCOM Dust Emission, Minimum-Median-Maximum ($Tg\,y^{-1}$)
Africa	57.1	935	220-804-3001
Asia S60	35.2	576	80-265-1253
Australia	0.7	11.3	9-31-129
Europe S60	0.2	3.5	
North America S60	1.9	31.4	1.7-2.0-286
South America	1.9	31.1	0.2-9.8-186
Eurasia N60	1.2	19.6	
Greenland	0.1	1.1	
Iceland	0.3	4.6	
North America N60	1.4	22.7	
Global		1636.3	514-1123-4313

[a]We also provide AEROCOM model estimates from *Huneeus et al.* [2011]. S60 indicates that only the area south of 60°N was included; N60 indicates that only the area north of 60°N was included.

Arabian Peninsula. These patterns are consistent with results shown by, e.g., *Zender et al.* [2003a] and *Ginoux et al.* [2001], although emission in Australia seems rather small. In combination with Figure 1, it appears that not much dust is mobilized at high northern latitudes. This is due to the influence of seasonal snow cover that inhibits dust emission during a part of the year. Furthermore, threshold changes due to soil moisture are more relevant in this region than in the main desert regions.

In Table 1 we split the total emission in different source regions. *Huneeus et al.* [2011] has given an overview of modeled dust emission from several regions. The regions defined here do not agree with *Huneeus et al.* [2011] since we are especially interested in near-Arctic source regions. However, for regions that are comparable, we added AEROCOM model estimates to Table 1. For all regions available, our estimates are in the range of the emission estimates presented by *Huneeus et al.* [2011]. It appears that estimated emissions in Australia are rather low in our simulations, as we already expected from Figure 2. This may be due to the land cover data set we use, where hardly any bare soil is assigned in Australia. For other regions, emission estimates are somewhat larger than the AEROCOM median values.

Table 1 further shows that dust emissions in regions north of 60°N are potentially large. In the studied years, they account for 1.7 to 5.3% of global dust emission, despite the inhibition of dust mobilization due to the seasonal snow cover. This is a large fraction of global dust emission, especially when considering that the area of this region is less than 7% of the area of the earth. Typical dust sources at high latitudes are proglacial fields or floodplains found, for example, in Alaska, Greenland, and Iceland, where fine glaciofluvial sediment deposits are exposed to wind. The seasonality of dust storms in these fields is different per source as it depends on snow cover, discharge, sediment supply, and wind speeds [e.g., *Crusius et al.,* 2011; *Arnalds et al.,* 2016; *Bullard et al.,* 2016]. The estimated dust emission from high latitudes in the Northern Hemisphere is comparable to a review study of *Bullard et al.* [2016] estimating that 5% of global dust emission is emitted from sources south of 40°S and north of 50°N. Their estimates for emission in northern high latitudes only include emissions from Iceland and Alaska and results in approximately 2% of global emitted dust. Furthermore, the FLEXDUST estimated dust emission north of 60°N ($48\,Tg\,yr^{-1}$) is considerably larger than the model estimate ($21.54\,Tg\,yr^{-1}$) of *Andersen et al.* [1998] for the region north of 47°N. Reasons for this difference may be found in model resolution ($5.6° \times 3.8°$ in their case), source definition and boundary layer parameterizations. Our annual emission for Iceland (varying from 1.9 to $9.9\,Tg\,yr^{-1}$ with a mean of $4.6\,Tg\,yr^{-1}$) is considerably lower than estimates of *Arnalds et al.* [2016] of 30 to $40\,Tg\,yr^{-1}$ based on dust storm frequency, detailed dust amount estimates from observations during a selection of storms and extrapolation of deposition maps [*Arnalds et al.,* 2014]. This may indicate that our high-latitude dust emissions for the Northern Hemisphere are conservative, probably underestimating real emissions.

The shown dust emission estimates and their good agreement with other model estimates suggest that the combination of the land cover data, mobilization scheme and meteorological model are adequate for dust mobilization estimates on these scales.

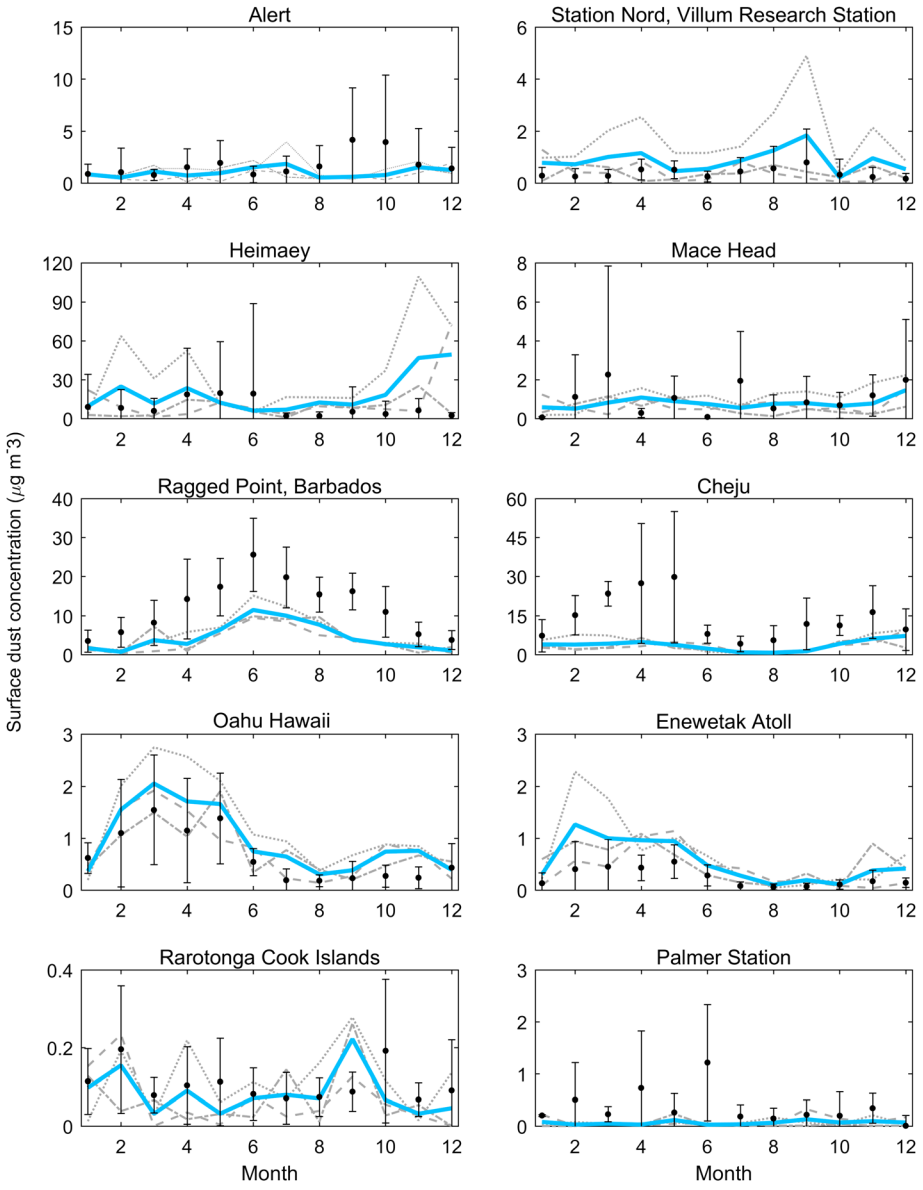

Figure 3. Monthly mean dust concentration (μg/m^3) at ten stations. The figure includes monthly means of observations (black) for the periods indicated in section 2.3 and simulations (grey and blue) for 2010 to 2012. Monthly mean values were estimated based on simulations in 2010 (grey dotted line), 2011 (grey dashed line), and 2012 (grey, dash-dotted line) and averaged over these three years (blue line).

3.2. Transport Model Evaluation

Observations that can be used for global dust transport model evaluation are limited, especially in our region of interest—the Arctic. We here chose to compare modeled monthly mean surface concentrations to observations. Note that the periods of measurements are different for each station and do not correspond to the modeled period. Results for several stations are shown in Figure 3.

From Figure 3 it is clear that the model does not perform equally well for all stations. We are mainly interested in the stations near the Arctic. Unfortunately, their number is limited. First, according to the observations, our model is able to capture the mean dust concentration at station Alert. However, the distinct increase of dust concentrations observed in autumn is not captured in any of the 3 years of simulations, similar to other model simulations [*Fan*, 2013]. Peak timing in the activity of dust sources varies per region [e.g., *Bullard et al.,* 2016] and while some sources are active throughout the year, others distinctly peak in a particular season due to a

combination of several factors. For instance for the Gulf of Alaska, peaks in transport of glacial dust were reported in autumn, when fine sediments are available and water levels decrease [*Crusius et al.,* 2011]. It is thus likely that a local dust source, mostly active in autumn, is missing in simulations of dust surface concentrations at Alert. Also note that dust concentration values at Alert in autumn appear considerably smaller in a different observational data set for the years 2000 to 2006 [*Fan*, 2013].

At Villum Research Station, Station Nord in North Greenland, the simulated surface concentrations are much larger in 2010 than in 2011 and 2012. Monthly mean concentrations are therefore in the upper range of the measurements. The higher simulated dust concentrations in 2010 may be related to the introduction of improved soil moisture and snow analysis schemes in ECMWF model cycle 36r4 in late 2010. The seasonal variation, however, with increased dust concentrations in spring and late summer does appear to be captured by the model, and the simulated concentrations in the two latter years reproduce the measured values very well.

At Heimaey, on the other hand, a station relatively close to Icelandic sandur areas, the model estimates are overpredicting dust amounts compared to measurements. This difference may to a large extent be due to the measurement setup. The dust sampler is only activated for winds from east to southwest, capturing dust arriving from remote sources but not from Iceland, with exceptions due to changing wind directions. Dust events with dust of local origin are therefore not measured, and observations should be considered an underestimate of true mean concentrations. In early winter, over predictions are largest, and this may additionally be caused by depleted sediment supply or problems in snow cover and soil moisture estimates.

Further south, at Mace Head, where dust only arrives from remote regions, the model captures the monthly mean values well. The signals in seasonal variation are unclear. A station that is strongly affected by dust from remote sources is Barbados, where dust is mainly of Saharan origin [e.g., *Prospero*, 1999]. FLEXPART is able to capture the seasonal variation, with maximum dust concentrations in summer. Nonetheless, the model underestimates the observed dust concentrations by approximately a factor 3. Such deviations are common in transport models; see, for example, model results presented by *Huneeus et al.* [2011]. As we found underestimates of dust concentrations in Tenerife as well (not shown), a possible explanation is an underestimate of dust emissions in the Sahara. However, total dust emissions in Africa were in agreement with other model estimates. The underestimate of dust concentrations could thus also be related to emission location rather than amounts. It is also possible that dust removal during transport is overestimated or that elevated transport in the Saharan air layer is not well enough captured. For instance, *Dentener et al.* [1996] discussed a possible lack of a transport mode above the marine boundary layer in their model. There are also large uncertainties in wet deposition schemes depending on accurate cloud and precipitation information. Small deviations in particle trajectories and deposition estimates will accumulate and can cause large errors at remote stations such as Barbados.

Seasonal variations are also visible at Cheju, with reduced concentrations in summer. FLEXPART captures some of this variation but underestimates concentrations considerably. Further south at Enewetak Atoll, where concentrations are also strongly influenced by dust from Asian sources, model simulations reproduce seasonal variation and mean values correspond to observations. A similar result is seen in Hawaii, with increased dust concentrations in spring. Also at Rarotonga, surface concentrations are well reproduced by FLEXPART. Finally, at Palmer Station (Antarctica), modeled surface concentrations are within the range of observed values but generally underestimate observed dust concentration. Due to the large distance between this station and source regions for dust, mostly South America and Australia, there can be many reasons for poor model performance. We have noted before that dust emissions in Australia are probably underestimated, making this a plausible explanation for the underestimation. In South America, dust emissions are in the range of estimates from other models. The modeled annual mean dust concentration at Palmer station is 0.06 $\mu g\, m^{-3}$. Since the observed concentration is 0.35 $\mu g\, m^{-3}$, model performance at this station is similar to other dust transport models, where deviations up to an order of magnitude are not rare [see, e.g., *Huneeus et al.,* 2011].

Besides surface concentrations, dust deposition amounts are also a way to evaluate model estimates. We show annual dust deposition amounts at 84 sites in Figure 4. We omit exact site locations but include their region in this plot. Full information on the sites and measurement method are presented in the individual data sets [see *Huneeus et al*., 2011, and references therein]. As for surface concentrations, measurement periods vary and do not necessarily correspond to the simulated period. For the Atlantic region, we find a

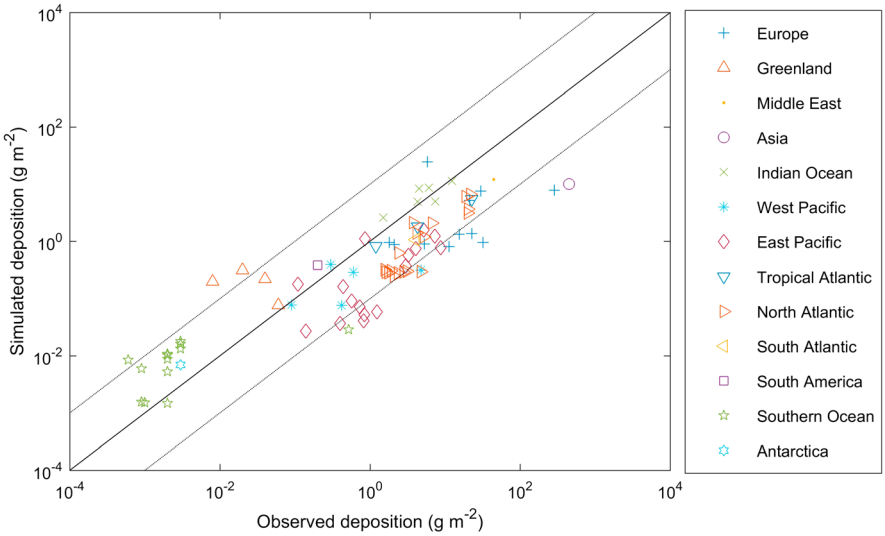

Figure 4. Modeled versus observed annual mean dust deposition (g m^{-2}) at 84 sites. See section 2.3 for details on the observations. The colors and markers indicate different regions.

general underestimation of deposition amounts compared to observations. In combination with the low surface concentration at Barbados, it thus appears that there is an underestimation of dust emission in the source region for dust in the Atlantic and Barbados or that dust is lifted to higher altitudes in our simulations. At the only observation site in Asia, Taklimakan, dust deposition is strongly underestimated. *Luo et al.* [2003] found a similar model result. They suggested that the coarse grid of the global model might be one of the reasons for the disagreement between model and observations. Especially for a site close to dust sources and in mountainous regions, sensitivity to model resolution may be large. Overall, model performance in estimating annual deposition is, with a correlation coefficient of 0.4 (or 0.9 for logarithmic values) and root mean square error of 57.3 g m^{-2}, similar to models presented in the AEROCOM comparison [*Huneeus et al.,* 2011] where the range of correlation coefficients was 0.08 (0.8) to 0.84 (0.92) and root-mean-square error varied from 31.4 to 58.3 g m^{-2} for a different model period than presented here.

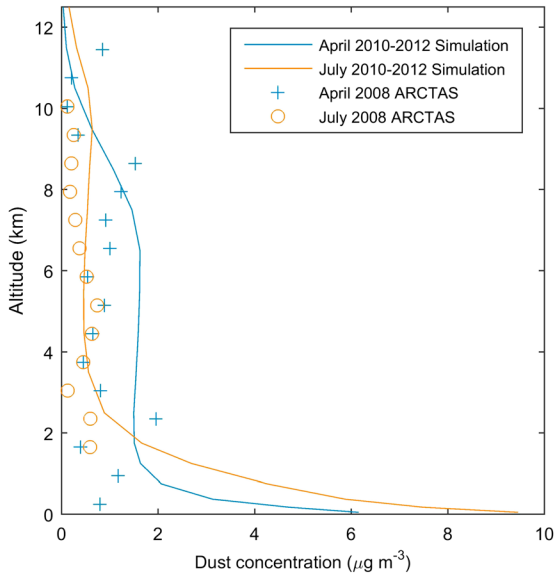

Figure 5. Monthly mean vertical profiles of dust concentrations in the high Arctic from model simulations (lines) and ARCTAS flight observations (plus and degree signs) in months April and July. Regions of interest for the flight campaigns differed in April and July. To capture the observation area, simulation profiles are averaged for the regions north of 60°N and 170°W to 35°W in April and 135°W to 35°W in July.

Finally, we evaluate the performance of the model considering concentrations at higher altitudes in the Arctic based on vertical profiles up to 12 km altitude measured during the ARCTAS flight campaigns (Figure 5) [*Jacob et al.,* 2010]. Since the simulation is done for different years than the observations, we do not sample the model exactly along the flight tracks. Rather, we extract average concentration profiles in the region where the aircraft flew to show whether vertical dust distribution is realistically simulated. The observations show that dust is present in the upper troposphere at high latitudes. We find similar dust concentrations in our simulations. In April, both in model and simulation, larger concentrations are seen at high altitudes (8 km) than lower

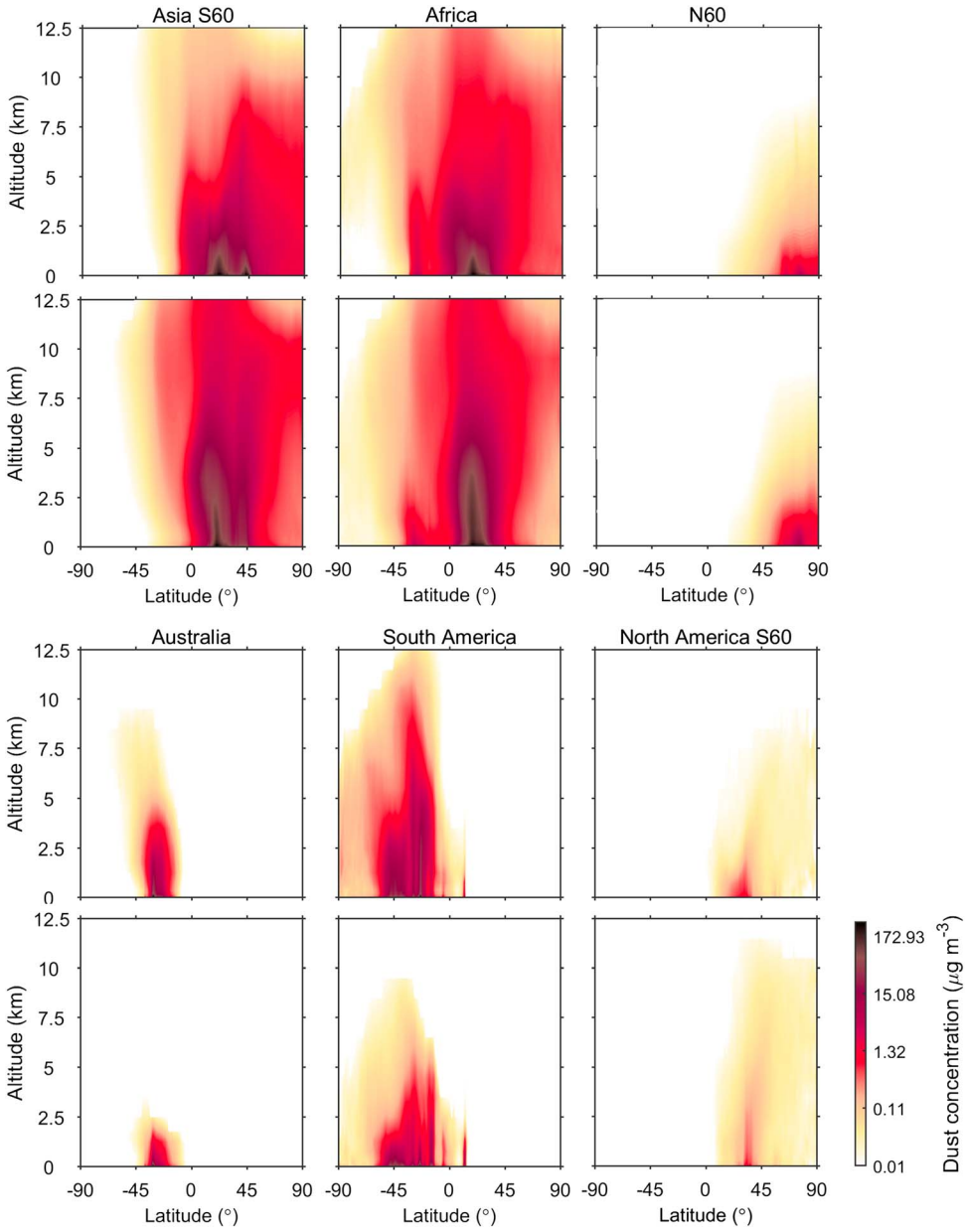

Figure 6. Seasonal mean dust concentration ($\mu g\, m^{-3}$) as a function of latitude and altitude for months December–February (rows 1 and 3) and June–August (rows 2 and 4) for simulations of different source regions. N60 combines the dust from all sources located north of 60°N.

in the troposphere. Near the surface, simulated dust concentrations appear larger in July than in April. This difference cannot be seen in observations since no near-surface measurements are available in July. Further discussion on seasonal variation in the Arctic will follow in section 3.4.

3.3. Simulated Dust Concentrations

The occurrence of dust in the atmosphere influences cloud formation and the radiation balance. The altitude of mineral aerosols will affect the influence they may have on such processes, as was for instance shown for radiative forcing due to black carbon [*Samset et al.,* 2013].

Figure 6 shows how mineral dust from six different source regions is distributed as a function of altitude and latitude. Dust from Asia and Africa can reach very high altitudes, while Asian dust is mostly confined to the Northern Hemisphere, African dust is also widely distributed in the Southern Hemisphere. In the Arctic,

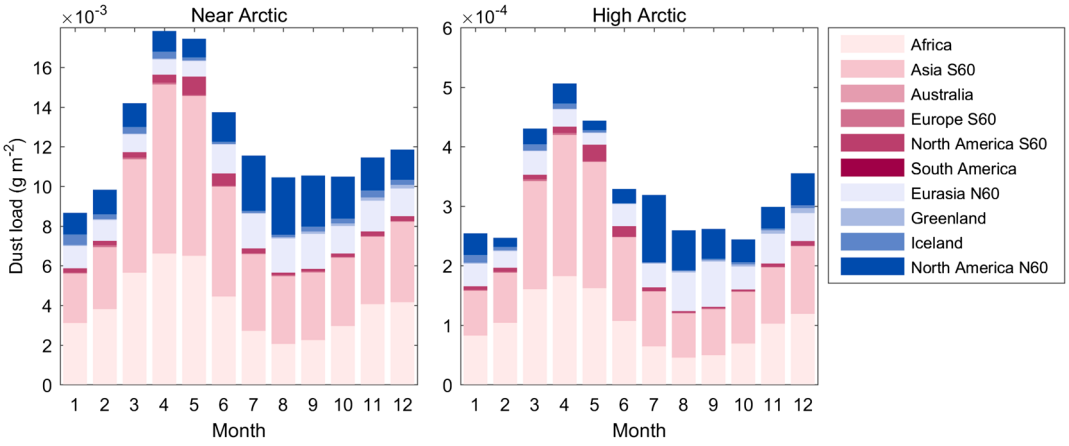

Figure 7. Monthly mean simulated (left) near Arctic (>60°N) and (right) high Arctic (>80°N) dust loads per source region. Red colors indicate remote sources; blue colors indicate high-latitude (Arctic) dust sources.

African and Asian dusts have higher concentrations in the upper troposphere than close to the surface. This is particularly evident in Figure 6 for African dust in summer. This distribution is consistent with slantwise lifting of air masses transported to the north, as warm air masses of southerly origin cannot intrude into the cold low-altitude air masses of the polar dome [*Stohl*, 2006]. Similar transport patterns have also been found for air pollution transport into the Arctic [e.g., *Heidam et al.,* 2004; *Stohl*, 2006; *Massling et al.,* 2015].

On the other hand, dust originating from areas north of 60°N remains mainly at low altitudes and high latitudes. Therefore, in the Arctic, dust of local origin has higher concentrations near the surface than dust from more southerly source regions, even though the dust emissions in the Arctic are more than an order of magnitude smaller. In the upper troposphere most of the dust in the Arctic appears to be of Asian and African origin, as will be discussed in more detail in the next section.

The amount of dust emitted in North America south of 60°N that is transported to the Arctic is small (Figure 6). In the Southern Hemisphere, mineral dust from South America and Africa appears to be dominating. This may also be related to the likely underestimation of Australian dust emission. Mineral dust from Australia does reach the Antarctic in our simulations, yet seasonal mean values are lower than the minimum contour value (0.01 $\mu g\, m^{-3}$) represented in Figure 6.

3.4. Mineral Dust in the Arctic

Longitudinal average profiles of dust concentration as a function of latitude (Figure 6) showed that several sources of mineral dust influence dust concentrations in the Arctic at different altitudes and seasons. We investigate this seasonal variation of mineral dust in the Arctic based on monthly means of atmospheric dust load and concentration profiles and discuss deposition patterns.

3.4.1. Mineral Dust Load

Mineral dust load in the Arctic undergoes a strong seasonal cycle in our simulations, as evident from Figure 7. We find that the seasonal variation of dust loads in the near and high Arctic are similar. Total dust loads are larger in the near Arctic than in the high Arctic due to the shorter distance to dust sources. Peak values of dust load occur in spring, caused by increased transport of dust from remote sources (reddish tints in Figure 7). As also shown in Figure 6, dust transport to the Arctic is in summer only possible at high altitudes, whereas dust from sources such as Africa or Asia can also reach the lower Arctic troposphere during spring. The peak in dust load is thus related to more efficient transport in spring. This is a typical feature of the Arctic Haze phenomenon [*Stohl*, 2006]. Modeled dust loads originating from sources north of 60°N (blue tones in Figure 7), on the other hand, peak in autumn. Figure 7 furthermore indicates that dust from remote sources, specifically Asia and Africa, dominates dust loads in the Arctic, and this is quantified in Table 2.

Table 2 shows the atmospheric dust loads from the different source regions, both globally as well as for the near and high Arctic. Globally, dust load is dominated by dust from the African continent. In the Arctic, however, the contribution of African dust to annual mean dust load (32%, near Arctic) is comparable to the dust contribution from local sources (27%). Largest dust load amounts in the Arctic with a share of approximately

Table 2. Relative Contributions (%) of Different Source Regions to Annual Mean Global, Near-Arctic, and High-Arctic Mineral Dust Loads

	Global	Near Arctic, >60°N	High Arctic, >80°N
Africa	61.8	31.6	30.8
Asia, S60	34.6	38.2	38.3
Australia	0.3	0.0	0.0
Europe, S60	0.1	0.4	0.5
North America, S60	1.0	2.6	2.7
South America	1.1	0.0	0.0
Eurasia, N60	0.4	10.6	12.8
Greenland	0.0	0.6	0.7
Iceland	0.1	2.0	1.4
North America, N60	0.6	14.0	12.8

38%, however, appear to be due to Asian dust from regions south of 60°N. Asian dust has been identified early as an important component of Arctic haze [*Rahn et al.,* 1977], while more recent research on Arctic haze has emphasized the role of air pollutants [*Quinn et al.,* 2007].

3.4.2. Vertical Profiles

Vertical profiles of mineral dust are influenced by remote as well as local sources and show a seasonal variation, related to transport (Figures 6 and 7) and dust availability. We here discuss vertical dust profiles based on simulated mean profiles in May and November. The size distribution of dust as a function of altitude is shown in Figure 8 (left). We first of all find that dust particles are present throughout the troposphere and the largest dust concentrations are found in the smallest size bins simulated. The size distribution differs from the size distribution of emitted particles (equation (7)), as large particles are deposited quickly and most dust here are fine particles transported from remote sources to the Arctic. For dust particles smaller than 12 μm, we find peaks of concentration at low (up to 1 km) and high (around 8 km) altitude in May. The lower peak is caused by local dust and the upper by remote dust. In November, we find increased amounts of large particles at low altitudes. Combined with Figure 7, we know that this is local dust, the mobilization of which peaks in autumn according to our simulations, as was for instance also shown for particular regions in Alaska [*Crusius et al.,* 2011]. Even though dust from remote sources is able to reach the lower Arctic troposphere in late winter/spring (Figure 6), we still find a peak of total dust concentration at high altitudes in May (Figure 8, right). In November, total dust column loadings are smaller than in May, but dust concentrations at low altitudes are larger due to the contribution of local dust.

3.4.3. Surface Concentration

The vertical profiles (Figure 8) indicated that dust surface concentrations in the high Arctic are larger in November than in May. We can elaborate this with Figure 9, where the mean dust concentration for altitudes

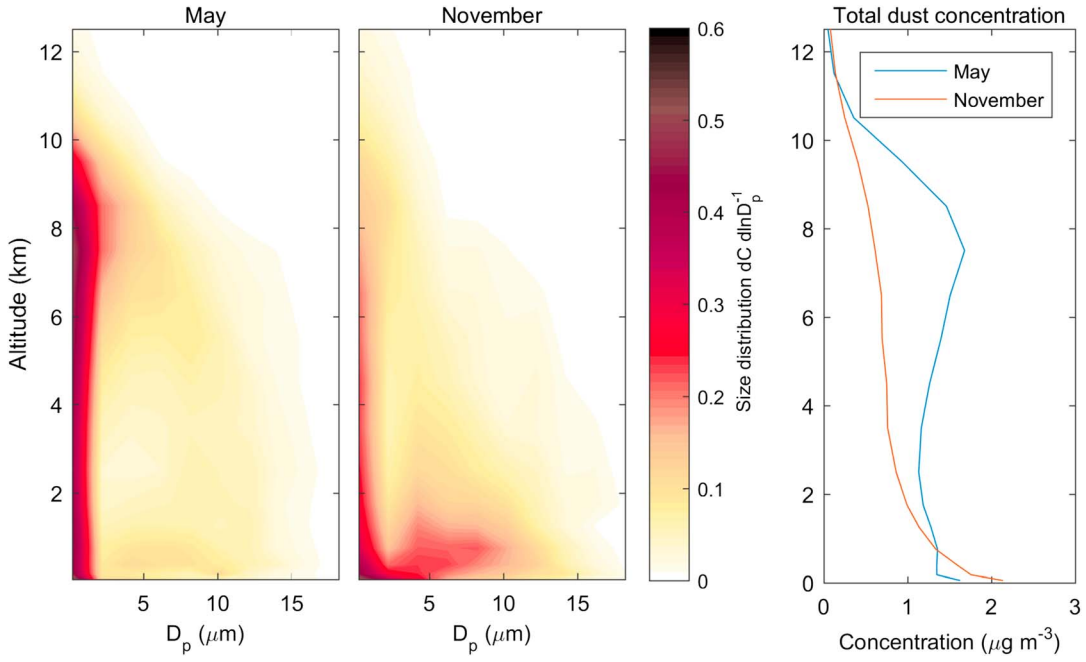

Figure 8. Size distribution of dust in the high Arctic as a function of altitude in (left) May and (middle) November, and (right) monthly mean total dust concentration in May and November.

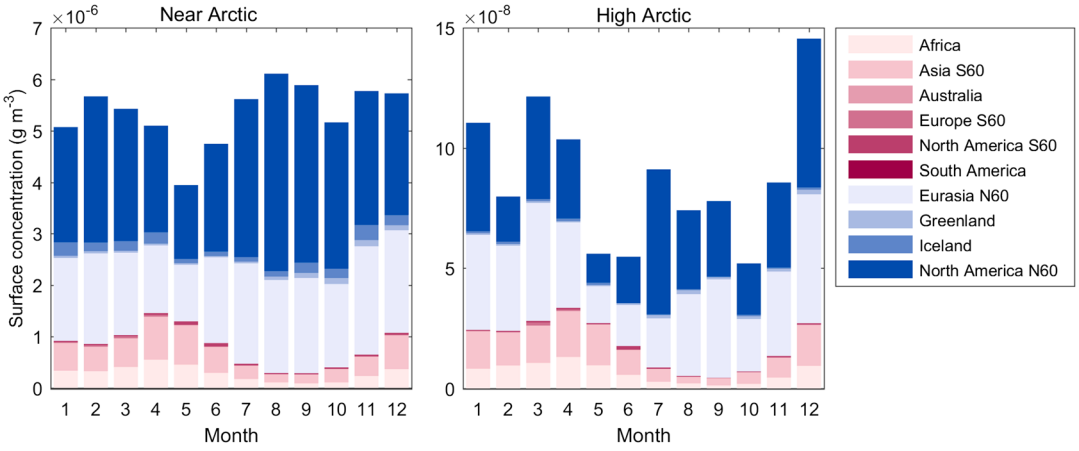

Figure 9. Monthly mean simulated surface concentrations of dust in the (left) near and (right) high Arctic per source region.

up to 100 m is shown. The seasonal variation of surface concentration appears to deviate much from the dust load annual cycle, especially in the near Arctic. As was suggested in Figure 6, dust from remote sources mostly reaches the lower Arctic troposphere in late winter/spring. The monthly values in Figure 9 confirm this, showing a minimum of dust surface concentrations from remote sources in summer/autumn. The presence of dust sources in the near Arctic causes dust from high latitudes to dominate modeled surface concentrations. The relative contributions from different source areas to the surface concentrations of dust in the Arctic (Table 3) are dramatically different from the total atmospheric dust loadings. At the surface, 85% of the near-Arctic dust originates from latitudes north of 60°N, whereas Asian dust contributes 9% and African dust only 5%. This clearly demonstrates the importance of high-latitude dust sources for Arctic surface dust concentrations. Similar results are obtained for dust deposition in the Arctic, shown in the next section.

3.4.4. Dust Deposition

While dust concentrations and dust loads can have important consequences for the radiative balance of the atmosphere and air quality, we are also interested in dust deposition. Deposition of dust can influence oceanic and terrestrial ecosystems by adding nutrients, or change the surface energy balance, especially of snow, ice sheets, and sea ice. Dust recorded in ice cores is also used as a tracer for climatic cycles [e.g., *Mayewski et al.,* 1994; *Lambert et al.,* 2008]. Before looking at the seasonal variation of dust deposition in detail, we look at the spatial patterns of dust deposition throughout the seasons (Figure 10).

Differences in the spatial pattern of dust deposition between the seasons are relatively small. Apparently, despite a seasonal snow cover, dust emission in the near Arctic is still important in winter, according to our simulations. Dust events in the Arctic have also been observed in winter [e.g., *Lewkowicz*, 1998; *Bullard*, 2013]. In the near Arctic simulated mean deposition amounts are largest in autumn. From Figure 10 it is clear that a large area is affected by dust deposition. The figure also indicates that dust deposition on the Greenland ice sheet occurs mostly in autumn and winter. The origin of this dust can help explain the seasonality. In Figure 11 we therefore show dust deposition in the Arctic from different regions. Deposition amounts are largest close to source regions, as, for instance, clearly seen for Icelandic dust sources. It even appears that dust originating from near Arctic sources does not travel far, compared to, for instance, Asian dust. More dust from Asia south of 60°N than from northern Eurasia reaches the Greenland ice sheet, for example. This is related not only to total emission

Table 3. Relative Contributions (%) of Different Sources Regions to Annual Mean Global, Near-Arctic, and High-Arctic Surface Dust Concentration

	Global	Near Arctic, >60°N	High Arctic, >80°N
Africa	60.8	5.2	7.4
Asia S60	33.6	8.9	13.3
Australia	0.4	0.0	0.0
Europe S60	0.1	0.3	0.3
North America S60	1.1	0.6	0.6
South America	1.0	0.0	0.0
Eurasia N60	1.1	31.9	38.5
Greenland	0.1	1.2	1.2
Iceland	0.1	3.2	0.8
North America N60	1.7	48.7	37.9

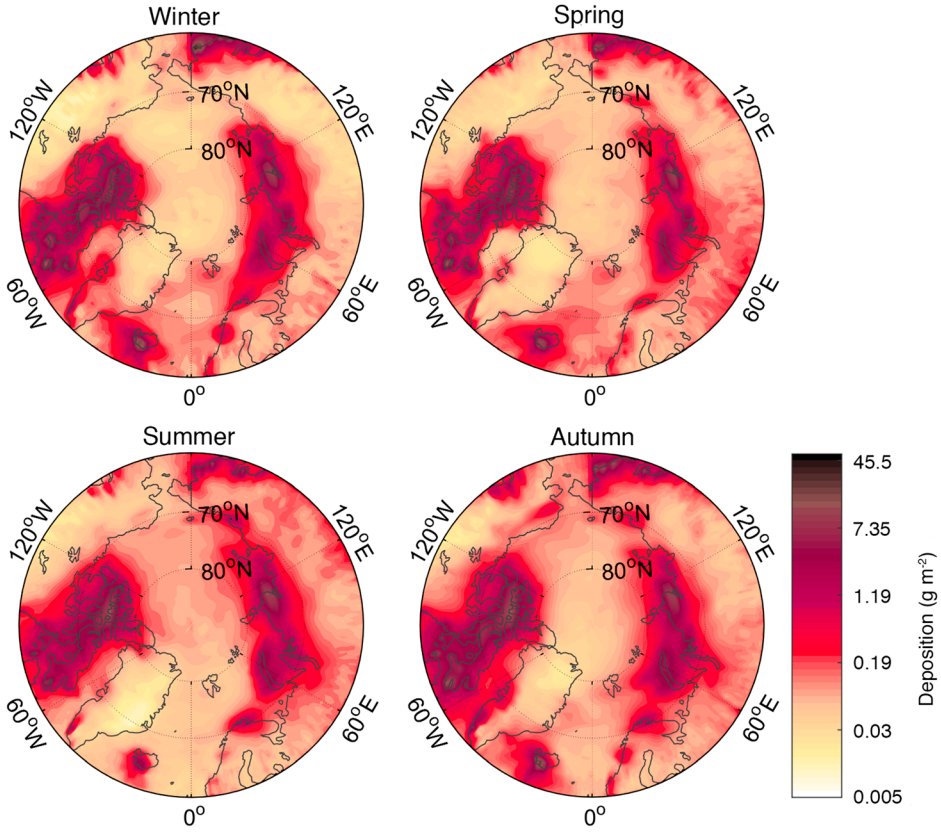

Figure 10. Simulated seasonal dust deposition (g m^{-2}) in the near Arctic averaged for years 2010–2012. Deposition is here given as the sum of dry and wet deposition.

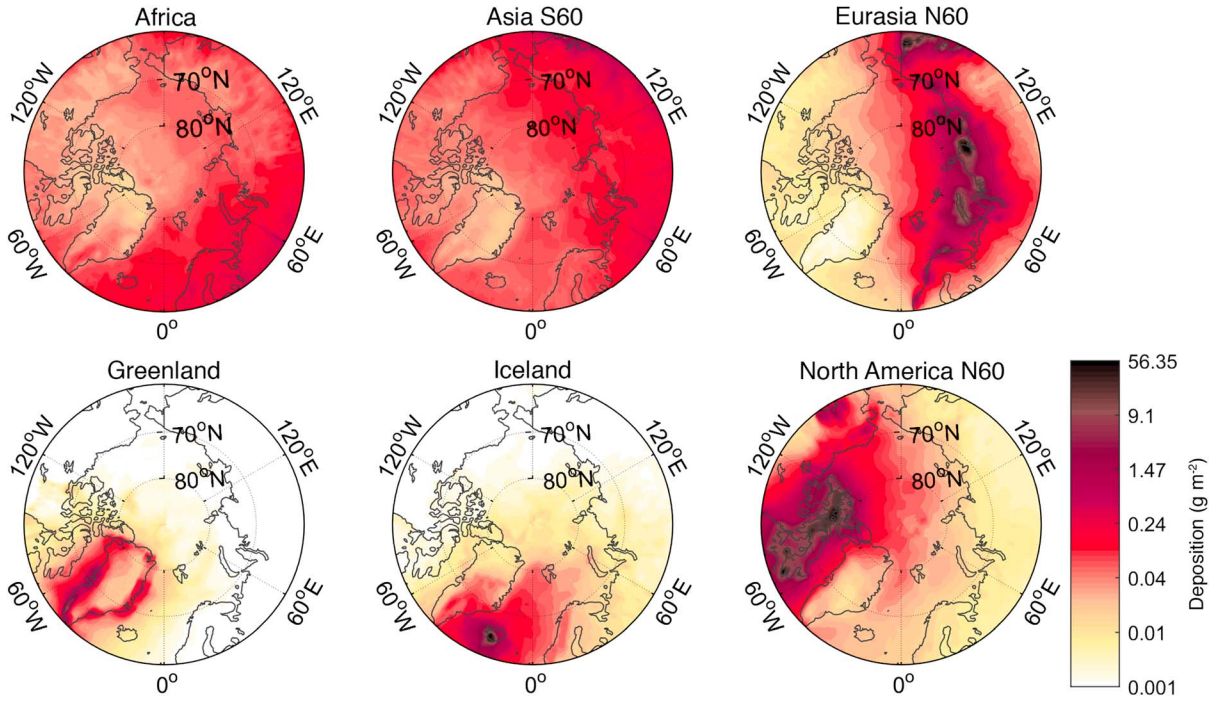

Figure 11. Simulated annual mean deposition of dust (g m^{-2}) in the near Arctic originating from different source regions averaged for years 2010−2012. Deposition is here given as the sum of dry and wet deposition.

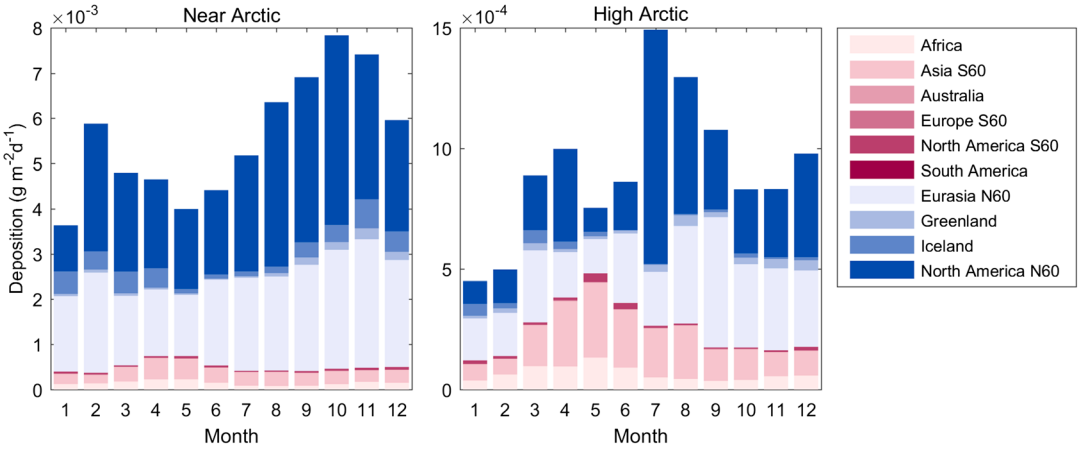

Figure 12. Monthly mean simulated dust deposition in the (left) near and (right) high Arctic per source region.

amounts but also to stronger convection at lower latitudes that causes dust to reach the upper troposphere and be transported over long distances. In contrast, near-Arctic dust remains mostly at altitudes lower than that of the Greenland ice sheet (also see Figure 6). The difference in travel distances also becomes apparent from dust lifetimes. With only 1.5 days, mean simulated lifetime of near-Arctic dust is smaller than global mean dust lifetime (about 4 days). Due to the high altitude of southern Asian and African dust in the Arctic, most of this dust is deposited through in-cloud and below-cloud scavenging.

In section 3.4.1 we showed that simulated atmospheric dust load in the Arctic peaks in spring. From Figure 10, however, we find that simulations do not confirm a peak of dust deposition in spring time. On the contrary, dust deposition peaks in autumn, as suggested in Figure 10 and clearly shown in Figure 12.

Contrary to dust load, the seasonal variation of dust deposition in the near Arctic differs considerably from the high Arctic. Largest modeled deposition occurs in autumn in the near Arctic, mostly due to deposition of dust from local sources. As discussed, main sources of dust at high latitudes are proglacial fields or floodplains that have largest dust emission in periods when dust is available, water levels are low, snow cover is discontinuous and wind speeds are high. Deposition of dust from remote sources does peak in spring, but values are small relative to total dust deposition. In the high Arctic remote sources add a larger contribution to dust deposition, but even here, local dust appears to dominate total dust deposition and the seasonal variation of deposition. The deposition of dust from remote sources peaks in spring, consistent with ice core observations from the Greenland ice sheet at high altitudes [e.g., *Gfeller et al.,* 2014], as will further be discussed below. We summarize the amounts of deposition in the Arctic in Table 4. We estimate that over 90% of the dust deposition in the near Arctic is of local origin. In the high Arctic, north of 80°N, and away from any significant dust source areas, this fraction is somewhat lower but still over 70% of deposited dust

Table 4. Relative Annual Mean Deposition (%) From Different Source Regions Globally and in Different Regions of the Arctic[a]

	Global	Near Arctic, >60°N	High Arctic, >80°N	Greenland	Greenland, > 2500 m	Sea Ice
Africa	57.8	3.6	10.2	6.4	22.8	5.6
Asia S60	35.9	5.5	18.0	4.9	13.0	10.1
Australia	0.5	0.0	0.0	0.0	0.0	0.0
Europe S60	0.1	0.2	0.3	0.1	0.1	0.1
North America S60	1.4	0.7	1.3	2.2	6.1	0.8
South America	1.3	0.0	0.0	0.0	0.0	0.0
Eurasia N60	1.2	35.9	30.2	1.1	1.3	11.5
Greenland	0.1	1.6	2.6	67.4	14.8	2.2
Iceland	0.2	5.8	2.0	9.0	33.6	1.3
North America N60	1.5	46.7	35.4	8.9	8.3	68.4

[a]Note that we did not account for a varying sea ice extent but used the sea ice extent of September 2012 [*Fetterer et al.,* 2002] to identify the sea ice region.

originates from source areas at high latitudes. Comparing this to the dust load amounts in Table 2, the contribution of African dust is small (10%). Even though there is relatively more dust from Africa and southern Asia in the Arctic upper troposphere, scavenging of this dust is much less efficient than that of the low-altitude dust of local origin.

These model results may initially appear contradictory to the results of ice core and snow pit studies at Summit, Greenland, showing considerable dust amounts originating from Asia [e.g., *Bory et al.,* 2003a]. However, one does need to consider that Summit is a high-altitude location. It is thus much more influenced by dust at higher altitudes than the Arctic on average. *Bory et al.* [2003b] included ice cores not only from high altitudes on the Greenland ice sheet but also from lower altitudes in their study. Results suggested that the lower cores, located closer to the ice margins, are influenced by proximal sources and experience more dust deposition than ice cores at higher altitudes. Moreover, *Wientjes et al.* [2011] studied samples of surface material at relatively low altitudes from a dark region in the western ablation zone of the Greenland ice sheet. Based on mineralogical composition, Asian deserts could be excluded as source regions of this material that was in part derived from outcropping ice. What is more, results suggested that the outcropping dust is likely of more local origin. Thus, to investigate the variation of dust source with altitude, we further included the relative contribution of different sources to dust deposition in Greenland and on the Greenland ice sheet only for grid points located higher than 2500 m in Table 4. For Greenland as a whole the model estimates that 67% of deposited dust originates from Greenland, but at high altitudes in Greenland this contribution is reduced to less than 15%. This demonstrates how near-Arctic dust is mostly deposited close to the source and hardly reaches high altitudes, as also discussed in section 3.4.1. In addition to the high atmospheric stability, which generally reduces vertical mixing in the Arctic, katabatic winds also inhibit upslope dust transport on Greenland. Some dust from Iceland is nonetheless able to reach the upper Greenland ice sheet in our simulations. Other strong contributors to dust in upper Greenland are Africa and Asia.

Results suggest that especially glaciers and snow covers at lower altitudes may be affected by dust. We therefore expect that sea ice albedo can also be influenced by dust deposition and do a similar analysis for the sea ice region. We here consider the sea ice region to be the region of the sea ice extent in September 2012 [*Fetterer et al.,* 2002]. In this region, we find the largest deposition contributions from sources in the near Arctic in North America, since these are the dust sources located closest to the sea ice (see Figure 2).

These results confirm the likely relevance of local dust sources as a factor influencing snow and ice albedo in the Arctic [*Dumont et al.,* 2014]. Obviously, the dynamic system of glaciofluvial sediment deposition, vegetation, aeolian transport, and deposition is complex and climate change can affect this in many ways, which we have not explored here. Nonetheless, we expect that a shortening of seasonal snow cover and potentially longer periods with dust emission in the near Arctic due to global warming are likely to affect snow and ice albedo at lower altitudes in the Arctic. Changes in dust emission in Asia and Africa and transport pathways are more likely to affect the Arctic cryosphere at higher altitudes.

4. Conclusions

A dust mobilization scheme has been developed to be used in combination with the Lagrangian particle dispersion model FLEXPART. A model evaluation based on monthly mean surface concentrations at several stations, vertical profiles of dust concentrations in the troposphere from aircraft observations, and annual mean deposition rates showed that the model is suitable for global dust transport simulations. A lack of dust observations in the Arctic was compensated by the use of aluminum concentrations to estimate dust concentrations. Although this conversion includes uncertainties, comparison of model and observations indicate that the model is also suitable to model mineral dust transport in the Arctic. With a series of global dust transport simulations, we could locate important dust sources for mineral dust in the Arctic.

Our results suggest that approximately 3% of global dust emission originates from the near-Arctic regions (>60°N). This estimate is close to a recent estimate of *Bullard et al.* [2016] suggesting that approximately 5% of global emitted dust is from sources south of 40°S and north of 50°N. Their estimates of northern high-latitudes only include Alaska and Iceland and result in approximately 2% of global emitted dust. Our 3% estimate that also includes other major dust sources (e.g., Eurasia) is thus similar, though all these estimates are uncertain. Uncertainties in dust emission estimates particularly in this region arise due to uncertainties of land cover and the large influence of snow cover and soil moisture on dust emissions. Additionally,

the interaction with glacial processes is currently difficult to account for on large scales. However, the large relative fraction of near-Arctic emissions compared to global emissions shows that dust emissions in these regions need more attention.

We also quantified the simulated total dust concentrations and dust deposition. From the results, it became clear that in the Arctic dust in the lower and upper troposphere must be considered separately. While near the surface, dust from local sources dominates concentrations (85%) and deposition (over 90%), in the total atmospheric column, dust from remote sources (mostly Asia and Africa, accounting for about 38% and 32%, respectively) is most important. The origin of deposited dust in ice cores is thus also strongly related to the altitude at which the ice cores were taken. At altitudes above 2500 m in Greenland, the model predicts relatively more dust deposition from Asia (13%) and Africa (23%) than at low altitudes (5% and 6%, respectively).

Results also clearly showed the strong seasonal cycle of dust occurrence in the Arctic. Especially, we found that different behavior is seen for dust deposition and atmospheric dust loads. Dust loads, dominated by dust from remote sources (over 72%), peak in spring due to enhanced transport. Surface concentrations controlled by local dust (over 85%) tend to be larger in autumn, although the seasonal cycle is less pronounced. Finally, dust deposition in the near Arctic is largest in autumn when more local dust is present, according to our simulations.

These estimates come with large uncertainties related to emission, cloud processes, and trajectories. In addition, model evaluation is less thorough in the Arctic due to a lack of dust concentration observations. However, considering the relevance of impurities for snow albedo and ice sheet melt [e.g., *Dumont et al.*, 2014] our results clearly indicate that efforts should be made to reduce these uncertainties and understand the processes behind dust emission and deposition at high latitudes. The estimated dust deposition and concentration amounts can, for instance, be used in future studies on the effects of dust on the radiation balance of the surface (snow and ice albedo) and the atmosphere (radiative forcing) and on nutrient transport to the ocean. Our study shows that it is of critical importance for such studies that near-Arctic dust sources, which hitherto were largely overlooked, are appropriately quantified.

Acknowledgments

We thank O. Arnalds and S. Helgi Brink for providing the soil-type map of Iceland. We thank S. Eckhardt, H. Sodemann, and A. Grini for their help. We thank J. Prospero for sharing data from station Heimaey. The data set from Station Alert used in this project has been reported to the AMAP monitoring program and is openly available from the database infrastructure EBAS (http://ebas.nilu.no/) hosted at NILU. We thank Environment Canada (L. Barrie) for providing their data. Finally, we thank NASA (M. Shook) for providing the ARCTAS flight campaign data. We acknowledge the Swiss National Science Foundation (SNF) for funding this project (155294). Travel grants have been provided by Nordic Center of Excellence eSTICC (Nordforsk 57001) and CRAICC (Nordforsk). The activities at Villum Research Station were financially supported by the Danish Environmental Protection Agency with means from the MIKA/DANCEA funds for Environmental Support to the Arctic Region, which is part of the Danish contribution to "Arctic Monitoring and Assessment Program" (AMAP). FLEXPART source code is available from www.flexpart.eu; model output data are available from the authors upon request.

References

Andersen, K. K., A. Armengaud, and C. Genthon (1998), Atmospheric dust under glacial and interglacial conditions, *Geophys. Res. Lett.*, *25*, 2281–2284, doi:10.1029/98GL51811.

Arimoto, R., R. A. Duce, B. J. Ray, W. G. Ellis, J. D. Cullen, and J. T. Merrill (1995), Trace-elements in the atmosphere over the North-Atlantic, *J. Geophys. Res.*, *100*, 1199–1213, doi:10.1029/94JD02618.

Arnalds, O. (2010), Dust sources and deposition of aeolian materials in Iceland, *Icel. Agric. Sci.*, *23*, 3–21.

Arnalds, O. (2015), *The Soils of Iceland*, 160 pp., Springer, Dordrecht, Netherlands.

Arnalds, O., H. Ólafsson, and P. Dagsson-Waldhauserova (2014), Quantification of iron-rich volcanogenic dust emissions and deposition over the ocean from Icelandic dust sources, *Biogeosciences*, *11*(23), 6623–6632.

Arnalds, O., P. Dagsson-Waldhauserova, and H. Olafsson (2016), The Icelandic volcanic aeolian environment: Processes and impacts—A review, *Aeolian Res.*, *20*, 176–195, doi:10.1016/j.aeolia.2016.01.004.

Biscaye, P. E., F. E. Grousset, M. Revel, S. VanderGaast, G. A. Zielinski, A. Vaars, and G. Kukla (1997), Asian provenance of glacial dust (stage 2) in the Greenland Ice Sheet Project 2 Ice Core, Summit, Greenland, *J. Geophys. Res.*, *102*, 26,765–26,781, doi:10.1029/97JC01249.

Bory, A. J. M., P. E. Biscaye, A. Svensson, and F. E. Grousset (2002), Seasonal variability in the origin of recent atmospheric mineral dust at NorthGRIP, Greenland, *Earth Planet. Sci. Lett.*, *196*(3–4), 123–134, doi:10.1016/S0012-821X(01)00609-4.

Bory, A. J. M., P. E. Biscaye, and F. E. Grousset (2003a), Two distinct seasonal Asian source regions for mineral dust deposited in Greenland (NorthGRIP), *Geophys. Res. Lett.*, *30*(4), 1167, doi:10.1029/2002GL016446.

Bory, A. J. M., P. E. Biscaye, A. Piotrowski, and J. P. Steffensen (2003b), Regional variability of ice core dust composition and provenance in Greenland, *Geochem. Geophys. Geosyst.*, *4*(12), 1107, doi:10.1029/2003GC000627.

Boussetta, S., G. Balsamo, A. Beljaars, T. Kral, and L. Jarlan (2013), Impact of a satellite-derived leaf area index monthly climatology in a global numerical weather prediction model, *Int. J. Remote Sens.*, *34*(9-10), 3520–3542, doi:10.1080/01431161.2012.716543.

Breider, T. J., L. J. Mickley, D. J. Jacob, Q. Wang, J. A. Fisher, R. Chang, and B. Alexander (2014), Annual distributions and sources of Arctic aerosol components, aerosol optical depth, and aerosol absorption, *J. Geophys. Res. Atmos.*, *119*, 4107–4124, doi:10.1002/2013JD020996.

Bullard, J. E. (2013), Contemporary glacigenic inputs to the dust cycle, *Earth Surf. Processes Landforms*, *38*(1), 71–89, doi:10.1002/esp.3315.

Bullard, J. E., and M. J. Austin (2011), Dust generation on a proglacial floodplain, West Greenland, *Aeolian Res.*, *3*(1), 43–54, doi:10.1016/j.aeolia.2011.01.002.

Bullard, J. E., et al. (2016), High latitude dust in the Earth system, *Rev. Geophys.*, *54*, 447–485, doi:10.1002/2016RG000518.

Crusius, J., A. W. Schroth, S. Gasso, C. M. Moy, R. C. Levy, and M. Gatica (2011), Glacial flour dust storms in the Gulf of Alaska: Hydrologic and meteorological controls and their importance as a source of bioavailable iron, *Geophys. Res. Lett.*, *38*, L06602, doi:10.1029/2010GL046573.

Dagsson-Waldhauserova, P., O. Arnalds, and H. Olafsson (2014a), Long-term variability of dust events in Iceland (1949–2011), *Atmos. Chem. Phys.*, *14*, 13,411–13,422, doi:10.5194/acp-14-13411-2014.

Dagsson-Waldhauserova, P., O. Arnalds, H. Olafsson, L. Skrabalova, G. M. Sigurdardottir, M. Branis, J. Hladil, R. Skala, T. Navratil, and L. Chadimova (2014b), Physical properties of suspended dust during moist and low wind conditions in Iceland, *Icel. Agric. Sci.*, *27*, 25–39.

Dentener, F. J., G. R. Carmichael, Y. Zhang, J. Lelieveld, and P. J. Crutzen (1996), Role of mineral aerosol as a reactive surface in the global troposphere, *J. Geophys. Res.*, *101*, 22,869–22,889, doi:10.1029/96JD01818.

Dumont, M., E. Brun, G. Picard, M. Michou, Q. Libois, J. Petit, M. Geyer, S. Morin, and B. Josse (2014), Contribution of light-absorbing impurities in snow to Greenland's darkening since 2009, *Nat. Geosci.*, *7*(7), 509–512, doi:10.1038/ngeo2180.

Eckhardt, S., A. Stohl, S. Beirle, N. Spichtinger, P. James, C. Forster, C. Junker, T. Wagner, U. Platt, and S. Jennings (2003), The North Atlantic Oscillation controls air pollution transport to the Arctic, *Atmos. Chem. Phys.*, *3*(5), 1769–1778, doi:10.5194/acp-3-1769-2003.

Fan, S.-M. (2013), Modeling of observed mineral dust aerosols in the arctic and the impact on winter season low-level clouds, *J. Geophys. Res. Atmos.*, *118*, 11,161–11,174, doi:10.1002/jgrd.50842.

Fécan, F., B. Marticorena, and G. Bergametti (1999), Parametrization of the increase of the aeolian erosion threshold wind friction velocity due to soil moisture for arid and semi-arid areas, *Ann. Geophys.*, *17*(1), 149–157, doi:10.1007/s00585-999-0149-7.

Fetterer, F., K. Knowles, W. Meier, M. Savoie (2002), Sea Ice Index [monthly dataset], NSIDC: National Snow and Ice Data Center, Boulder, Colo., doi:10.7265/N5QJ7F7W.

Fristrup, B. (1953), Wind erosion within the Arctic deserts, *Geogr. Tidsskr.*, *52*, 51–65.

Gfeller, G., H. Fischer, M. Bigler, S. Schüpbach, D. Leuenberger, and O. Mini (2014), Representativeness and seasonality of major ion records derived from NEEM firn cores, *Cryosphere*, *8*(5), 1855–1870, doi:10.5194/tc-8-1855-2014.

Ginoux, P., M. Chin, I. Tegen, J. M. Prospero, B. Holben, O. Dubovik, and S. J. Lin (2001), Sources and distributions of dust aerosols simulated with the GOCART model, *J. Geophys. Res.*, *106*, 20,255–20,273, doi:10.1029/2000JD000053.

Global Soil Data Task (2014), Global soil data products CD-ROM contents (IGBP-DIS), Data Set, Oak Ridge Natl. Lab. Distrib. Active Arch. Cent., Oak Ridge, Tenn., doi:10.3334/ORNLDAAC/565.

Griffin, D. W., and C. A. Kellogg (2004), Dust storms and their impact on ocean and human health: Dust in Earth's atmosphere, *EcoHealth*, *1*(3), 284–295, doi:10.1007/s10393-004-0120-8.

Grini, A., G. Myhre, C. S. Zender, and I. S. A. Isaksen (2005), Model simulations of dust sources and transport in the global atmosphere: Effects of soil erodibility and wind speed variability, *J. Geophys. Res.*, *110*, D02205, doi:10.1029/2004JD005037.

Grythe, H., N. I. Kristiansen, C. D. Groot Zwaaftink, S. Eckhardt, J. Ström, P. Tunved, R. Krejci, and A. Stohl (2016), A new aerosol wet removal scheme for the Lagrangian particle model FLEXPART, *Geosci. Model Dev. Discuss.*, 1–34, doi:10.5194/gmd-2016-267.

Hamilton, W. I., and C. C. Langway Jr. (1967), A correlation of microparticle concentrations with oxygen isotope ratios in 700 year old Greenland ice, *Earth Planet. Sci. Lett.*, *3*, 363–366.

Heidam, N. Z., J. Christensen, P. Wahlin, and H. Skov (2004), Arctic atmospheric contaminants in NE Greenland: Levels, variations, origins, transport, transformations and trends 1990–2001, *Sci. Total Environ.*, *331*(1-3), 5–28, doi:10.1016/j.scitotenv.2004.03.033.

Hirdman, D., H. Sodemann, S. Eckhardt, J. Burkhart, A. Jefferson, T. Mefford, P. Quinn, S. Sharma, J. Ström, and A. Stohl (2010), Source identification of short-lived air pollutants in the Arctic using statistical analysis of measurement data and particle dispersion model output, *Atmos. Chem. Phys.*, *10*(2), 669–693.

Huang, Z., J. Huang, T. Hayasaka, S. Wang, T. Zhou, and H. Jin (2015), Short-cut transport path for Asian dust directly to the Arctic: A case study, *Environ. Res. Lett.*, *10*(11), 11,4018–11,4026, doi:10.1088/1748-9326/10/11/114018.

Huneeus, N., et al. (2011), Global dust model intercomparison in AEROCOM phase I, *Atmos. Chem. Phys.*, *11*(15), 7781–7816, doi:10.5194/acp-11-7781-2011.

Iversen, J. D., and B. R. White (1982), Saltation threshold on Earth, Mars and Venus, *Sedimentology*, *29*(1), 111–119, doi:10.1111/j.1365-3091.1982.tb01713.x.

Jacob, D. J., et al. (2010), The Arctic Research of the Composition of the Troposphere from Aircraft and Satellites (ARCTAS) mission: Design, execution, and first results, *Atmos. Chem. Phys.*, *10*(11), 5191–5212, doi:10.5194/acp-10-5191-2010.

Kang, J.-H., H. Hwang, S. B. Hong, S. Do Hur, S.-D. Choi, J. Lee, and S. Hong (2015), Mineral dust and major ion concentrations in snowpit samples from the NEEM site, Greenland, *Atmos. Environ.*, *120*, 137–143, doi:10.1016/j.atmosenv.2015.08.062.

Kim, H., and M. Choi (2015), Impact of soil moisture on dust outbreaks in East Asia: Using satellite and assimilation data, *Geophys. Res. Lett.*, *42*, 2789–2796, doi:10.1002/2015GL063325.

Koehler, K. A., S. M. Kreidenweis, P. J. DeMott, M. D. Petters, A. J. Prenni, and O. Möhler (2010), Laboratory investigations of the impact of mineral dust aerosol on cold cloud formation, *Atmos. Chem. Phys.*, *10*(23), 11,955–11,968, doi:10.5194/acp-10-11955-2010.

Kohfeld, K. E., and S. P. Harrison (2001), DIRTMAP: The geological record of dust, *Earth Sci. Rev.*, *54*(1-3), 81–114, doi:10.1016/s0012-8252(01)00042-3.

Kok, J. F. (2011), A scaling theory for the size distribution of emitted dust aerosols suggests climate models underestimate the size of the global dust cycle, *Proc. Natl. Acad. Sci. U. S. A.*, *108*(3), 1016–1021, doi:10.1073/pnas.1014798108.

Kok, J. F., E. J. R. Parteli, T. I. Michaels, and D. B. Karam (2012), The physics of wind-blown sand and dust, *Rep. Prog. Phys.*, *75*(10), 106,901.

Lambert, F., B. Delmonte, J. R. Petit, M. Bigler, P. R. Kaufmann, M. A. Hutterli, T. F. Stocker, U. Ruth, J. P. Steffensen, and V. Maggi (2008), Dust-climate couplings over the past 800,000 years from the EPICA Dome C ice core, *Nature*, *452*(7187), 616–619, doi:10.1038/nature06763.

Lambert, F., A. Tagliabue, G. Shaffer, F. Lamy, G. Winckler, L. Farias, L. Gallardo, and R. De Pol-Holz (2015), Dust fluxes and iron fertilization in Holocene and Last Glacial Maximum climates, *Geophys. Res. Lett.*, *42*, 6014–6023, doi:10.1002/2015GL064250.

Lewkowicz, A. G. (1998), Aeolian sediment transport during winter, Black Top Creek, Fosheim Peninsula, Ellesmere Island, Canadian Arctic, *Permafrost Periglacial Processes*, *9*(1), 35–46.

Liu, M., D. L. Westphal, S. Wang, A. Shimizu, N. Sugimoto, J. Zhou, and Y. Chen (2003), A high-resolution numerical study of the Asian dust storms of April 2001, *J. Geophys. Res.*, *108*(D23), 8653, doi:10.1029/2002JD003178.

Luo, C., N. M. Mahowald, and J. del Corral (2003), Sensitivity study of meteorological parameters on mineral aerosol mobilization, transport, and distribution, *J. Geophys. Res.*, *108*(D15), 4447, doi:10.1029/2003JD003483.

Mahowald, N., K. Kohfeld, M. Hansson, Y. Balkanski, S. P. Harrison, I. C. Prentice, M. Schulz, and H. Rodhe (1999), Dust sources and deposition during the Last Glacial Maximum and current climate: A comparison of model results with paleodata from ice cores and marine sediments, *J. Geophys. Res.*, *104*, 15,895–15,916, doi:10.1029/1999JD900084.

Mahowald, N. M., S. Engelstaedter, C. Luo, A. Sealy, P. Artaxo, C. Benitez-Nelson, S. Bonnet, Y. Chen, P. Y. Chuang, and D. D. Cohen (2009), Atmospheric iron deposition: Global distribution, variability, and human perturbations, *Annu. Rev. Mar. Sci.*, *1*, 245–278.

Marticorena, B., and G. Bergametti (1995), Modeling the atmospheric dust cycle: 1. Design of a soil-derived dust emission scheme, *J. Geophys. Res.*, *100*, 16,415–16,430, doi:10.1029/95JD00690.

Massling, A., I. E. Nielsen, D. Kristensen, J. H. Christensen, L. L. Sorensen, B. Jensen, Q. T. Nguyen, J. K. Nojgaard, M. Glasius, and H. Skov (2015), Atmospheric black carbon and sulfate concentrations in Northeast Greenland, *Atmos. Chem. Phys.*, *15*(16), 9681–9692, doi:10.5194/acp-15-9681-2015.

Mayewski, P. A., et al. (1994), Changes in atmospheric circulation and ocean ice cover over the North Atlantic during the last 41,000 years, *Science*, *263*(5154), 1747–1751, doi:10.1126/science.263.5154.1747.
McKenna-Neuman, C., and W. G. Nickling (1989), A theoretical and wind tunnel investigation of the effect of capillary water on the entrainment of sediment by wind, *Can. J. Soil Sci.*, *69*(1), 79–96, doi:10.4141/cjss89-008.
Moore, J. K., S. C. Doney, and K. Lindsay (2004), Upper ocean ecosystem dynamics and iron cycling in a global three-dimensional model, *Global Biogeochem. Cycles*, *18*, GB4028, doi:10.1029/2004GB002220.
Näslund, E., and L. Thaning (1991), On the settling velocity in a nonstationary atmosphere, *Aerosol Sci. Technol.*, *14*(2), 247–256, doi:10.1080/02786829108959487.
Nguyen, Q., H. Skov, L. L. Sørensen, B. Jensen, A. G. Grube, A. Massling, M. Glasius, and J. K. Nøjgaard (2013), Source apportionment of particles at Station Nord, North East Greenland during 2008–2010 using COPREM and PMF analysis, *Atmos. Chem. Phys.*, *13*(1), 35–49.
Okin, G. S., N. Mahowald, O. A. Chadwick, and P. Artaxo (2004), Impact of desert dust on the biogeochemistry of phosphorus in terrestrial ecosystems, *Global Biogeochem. Cycles*, *18*, GB2005, doi:10.1029/2003GB002145.
Parajuli, S. P., Z. L. Yang, and G. Kocurek (2014), Mapping erodibility in dust source regions based on geomorphology, meteorology, and remote sensing, *J. Geophys. Res. Earth Surf.*, *119*, 1977–1994, doi:10.1002/2014JF003095.
Parajuli, S. P., T. M. Zobeck, G. Kocurek, Z. L. Yang, and G. L. Stenchikov (2016), New insights into the wind-dust relationship in sandblasting and direct aerodynamic entrainment from wind tunnel experiments, *J. Geophys. Res. Atmos.*, *121*, 1776–1792, doi:10.1002/2015JD024424.
Prospero, J. M. (1996), The atmospheric transport of particles to the ocean, in *Particle Flux in the Ocean, SCOPE*, vol. 57, edited by V. Ittekkot et al., 19–52, John Wiley, New York.
Prospero, J. M. (1999), Long-range transport of mineral dust in the global atmosphere: Impact of African dust on the environment of the southeastern United States, *Proc. Natl. Acad. Sci. U. S. A.*, *96*(7), 3396–3403, doi:10.1073/pnas.96.7.3396.
Prospero, J. M., M. Uematsu, and D. L. Savoie (1989), *Mineral Aerosol Transport to the Pacific Ocean*, Academic, New York.
Prospero, J. M., J. E. Bullard, and R. Hodgkins (2012), High-latitude dust over the North Atlantic: Inputs from Icelandic proglacial dust storms, *Science*, *335*(6072), 1078–1082, doi:10.1126/science.1217447.
Quinn, P. K., G. Shaw, E. Andrews, E. G. Dutton, T. Ruoho-Airola, and S. L. Gong (2007), Arctic haze: Current trends and knowledge gaps, *Tellus, Ser. B*, *59*(1), 99–114, doi:10.1111/j.1600-0889.2006.00238.x.
Rahn, K. A., R. D. Borys, and G. E. Shaw (1977), Asian source of Arctic haze bands, *Nature*, *268*(5622), 713–715, doi:10.1038/268713a0.
Ram, M., and G. Koenig (1997), Continuous dust concentration profile of pre-Holocene ice from the Greenland Ice Sheet Project 2 ice core: Dust stadials, interstadials, and the Eemian, *J. Geophys. Res.*, *102*, 26,641–26,648, doi:10.1029/96JC03548.
Samset, B. H., et al. (2013), Black carbon vertical profiles strongly affect its radiative forcing uncertainty, *Atmos. Chem. Phys.*, *13*(5), 2423–2434, doi:10.5194/acp-13-2423-2013.
Shao, Y., and H. Lu (2000), A simple expression for wind erosion threshold friction velocity, *J. Geophys. Res.*, *105*, 22,437–22,443, doi:10.1029/2000JD900304.
Sirois, A., and L. A. Barrie (1999), Arctic lower tropospheric aerosol trends and composition at Alert, Canada: 1980–1995, *J. Geophys. Res.*, *104*, 11,599–11,618, doi:10.1029/1999JD900077.
Sodemann, H., T. M. Lai, F. Marenco, C. L. Ryder, C. Flamant, P. Knippertz, P. Rosenberg, M. Bart, and J. B. McQuaid (2015), Lagrangian dust model simulations for a case of moist convective dust emission and transport in the western Sahara region during Fennec/LADUNEX, *J. Geophys. Res. Atmos.*, *120*, 6117–6144, doi:10.1002/2015JD023283.
Stohl, A. (2006), Characteristics of atmospheric transport into the Arctic troposphere, *J. Geophys. Res.*, *111*, D11306, doi:10.1029/2005JD006888.
Stohl, A., M. Hittenberger, and G. Wotawa (1998), Validation of the Lagrangian particle dispersion model FLEXPART against large-scale tracer experiment data, *Atmos. Environ.*, *32*(24), 4245–4264, doi:10.1016/S1352-2310(98)00184-8.
Stohl, A., S. Eckhardt, C. Forster, P. James, and N. Spichtinger (2002), On the pathways and timescales of intercontinental air pollution transport, *J. Geophys. Res.*, *107*(D23), 4684, doi:10.1029/2001JD001396.
Stohl, A., C. Forster, A. Frank, P. Seibert, and G. Wotawa (2005), Technical note: The Lagrangian particle dispersion model FLEXPART version 6.2, *Atmos. Chem. Phys.*, *5*(9), 2461–2474.
Stohl, A., Z. Klimont, S. Eckhardt, and K. Kupiainen (2013), Why models struggle to capture Arctic Haze: The underestimated role of gas flaring and domestic combustion emissions, *Atmos. Chem. Phys. Discuss.*, *13*(4), 9567–9613, doi:10.5194/acpd-13-9567-2013.
Stone, R. S., G. P. Anderson, E. Andrews, E. G. Dutton, E. P. Shettle, and A. Berk (2007), Incursions and radiative impact of Asian dust in northern Alaska, *Geophys. Res. Lett.*, *34*, L14815, doi:10.1029/2007GL029878.
Tateishi, R., N. T. Hoan, T. Kobayashi, B. Alsaaideh, G. Tana, and D. X. Phong (2014), Production of Global Land Cover Data-GLCNMO2008, *J. Geogr. Geol.*, *6*(3), 99.
Tegen, I., and I. Fung (1994), Modeling of mineral dust in the atmosphere: Sources, transport, and optical thickness, *J. Geophys. Res.*, *99*, 22,897–22,914, doi:10.1029/94JD01928.
Tegen, I., S. P. Harrison, K. Kohfeld, I. C. Prentice, M. Coe, and M. Heimann (2002), Impact of vegetation and preferential source areas on global dust aerosol: Results from a model study, *J. Geophys. Res.*, *107*(D21), 4576, doi:10.1029/2001JD000963.
Uno, I., et al. (2003), Regional chemical weather forecasting system CFORS: Model descriptions and analysis of surface observations at Japanese island stations during the ACE-Asia experiment, *J. Geophys. Res.*, *108*(D23), 8668, doi:10.1029/2002JD002845.
VanCuren, R. A., T. Cahill, J. Burkhart, D. Barnes, Y. Zhao, K. Perry, S. Cliff, and J. McConnell (2012), Aerosols and their sources at Summit Greenland—First results of continuous size- and time-resolved sampling, *Atmos. Environ.*, *52*, 82–97, doi:10.1016/j.atmosenv.2011.10.047.
Warren, S. G., and W. J. Wiscombe (1980), A model for the spectral albedo of snow. II: Snow containing atmospheric aerosols, *J. Atmos. Sci.*, *37*(12), 2734–2745, doi:10.1175/1520-0469(1980)037<2734:AMFTSA>2.0.CO;2.
Wientjes, I., R. Van de Wal, G.-J. Reichart, A. Sluijs, and J. Oerlemans (2011), Dust from the dark region in the western ablation zone of the Greenland ice sheet, *Cryosphere*, *5*(3), 589–601, doi:10.5194/tc-5-589-2011.
Yin, Y., S. Wurzler, Z. Levin, and T. G. Reisin (2002), Interactions of mineral dust particles and clouds: Effects on precipitation and cloud optical properties, *J. Geophys. Res.*, *107*(D23), 4724, doi:10.1029/2001JD001544.
Zdanowicz, C. M., G. A. Zielinski, and C. P. Wake (1998), Characteristics of modern atmospheric dust deposition in snow on the Penny Ice Cap, Baffin Island, Arctic Canada, *Tellus, Ser. B*, *50*(5), 506–520, doi:10.1034/j.1600-0889.1998.t01-1-00008.x.
Zender, C. S., H. Bian, and D. Newman (2003a), Mineral Dust Entrainment and Deposition (DEAD) model: Description and 1990s dust climatology, *J. Geophys. Res.*, *108*(D14), 4416, doi:10.1029/2002JD002775.
Zender, C. S., D. Newman, and O. Torres (2003b), Spatial heterogeneity in aeolian erodibility: Uniform, topographic, geomorphic, and hydrologic hypotheses, *J. Geophys. Res.*, *108*(D17), 4543, doi:10.1029/2002JD003039.